7. Experimental observations (laboratory) of circulating elastic waves in rock

7.1 Elastic constants of the granite

Experiments were conducted on the inner surface of a 150mm-diameter , diamond-drilled, borehole in a large Harcourt granite block. The granite block was 1m x 1m x 2m in size and approximately 5 $x10^3$ kg in mass. The block had been the subject of extensive dynamic elastic experiments (to be reported at a later date) and thus the bulk dynamic elastic properties were reasonably well established. The dynamic elastic properties for the Harcourt granite are as follows:

Elastic properties deduced from fundamental vibrational resonance experiments (longitudinal, torsional and flexural resonances of the block were measured) together with supporting 3-dimensional, dynamic finite-element eigenfrequency analyses. (These experiments will be reported in Blair, Siggins and Coulthard, 1988, in preparation; however, agreement between experiment and DFEM was of the order of 2%.)

Dynamic Young's modulus	4.8×10^{10} Pa
Poisson's ratio	0.25
Lame' elastic constants, ($\lambda = \mu$)	1.92×10^{10} Pa
Density	2.66×10^3 kg/m^3

Inferred wave phase velocities from the above properties,

Longitudinal wave velocity	4653 m/s
shear wave velocity	2686 m/s
Rayleigh wave velocity	2470 m/s

Measured wave velocities on the block using Panametric P and S type piezo-electric elements.

Longitudinal wave velocity	4690 m/s
shear wave velocity	2924 m/s
Rayleigh wave velocity	2580 m/s

The above properties have an uncertainty of the order of ±5% due to experimental error and variations of velocity within the block. Lame' elastic constants deduced from the longitudinal and shear wave velocities are $\mu = 2.27 \times 10^{10}$ and $\lambda = 1.28 \times 10^{10}$ Pa. This implies a Poisson's ratio, ν, of 0.18 ($\nu = \lambda/2(\lambda + \mu)$). The compressional and Rayleigh wave velocities yield $\nu = 0.20$. Thus, the average value of ν from these tests is 0.19 which is at variance with the value of ν equal to 0.25 determined from resonance tests on the block. However, the discrepancy between dynamic moduli measured in wave velocity measurements and other test such as, vibrational resonance and static elastic tests is well known -- see Thill and Peng (1974), Siggins (1986) for example.

7.2 Measurements on circulating elastic waves around test cross-sections in a borehole

Initial experiments on circulating waves were conducted on a central cross-section of the centre borehole. The central hole was chosen in order to maximise the distance from the free surfaces of the block so that the possibility of unwanted reflections from these surfaces would be reduced. Figure 29(a) and (b) illustrate the instrumented block and Figure 30 is a schematic diagram of the instrumentation.

Acoustic sources used in these experiments were constructed from discs of piezo-electric material, 3mm in thickness, with silvered faces constructed to respond in the thickness mode of vibration. The piezo-electric material was a modified Lead Zirconate-

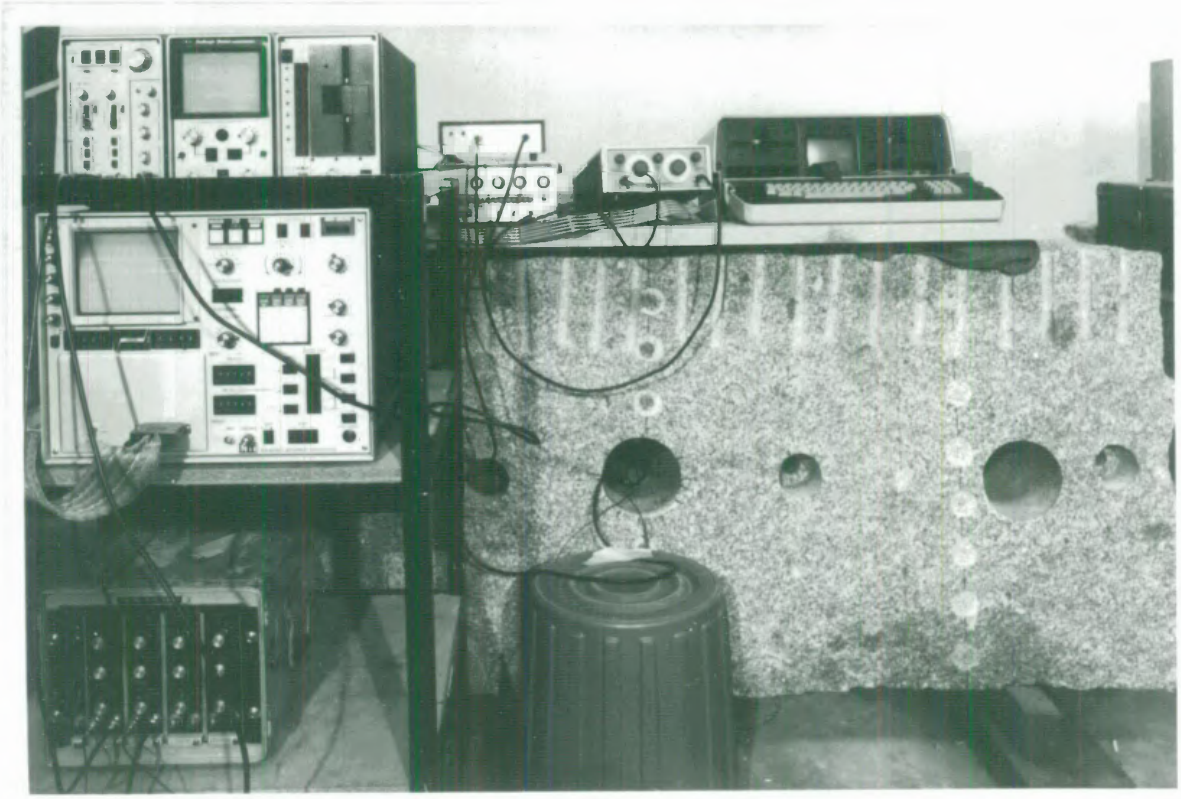

(a)

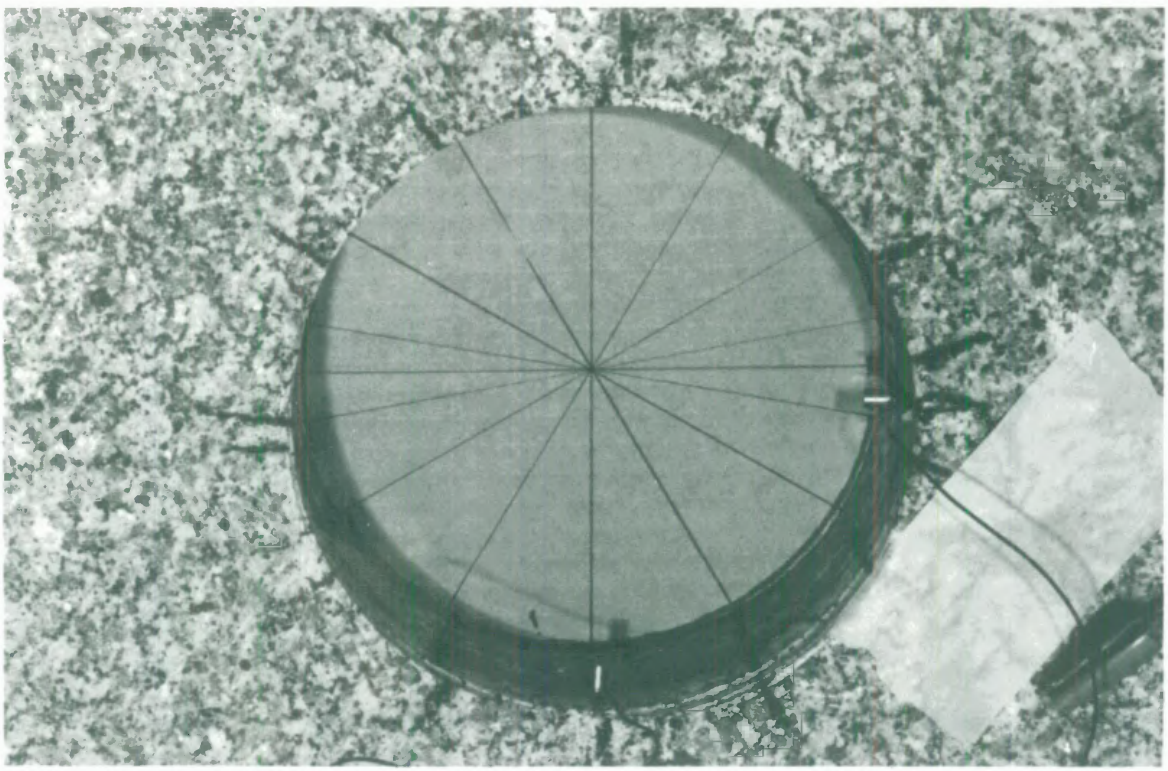

(b)

Figure 29 (a). Instrumentation of a bore-hole in a Harcourt granite block; (b) accelerometers and piezo-electric source in position on the test cross-section. The source is located on the right-hand side of the cavity wall (3 o'clock position) together with an accelerometer on the back of the source. The detector accelerometer is at -90°.

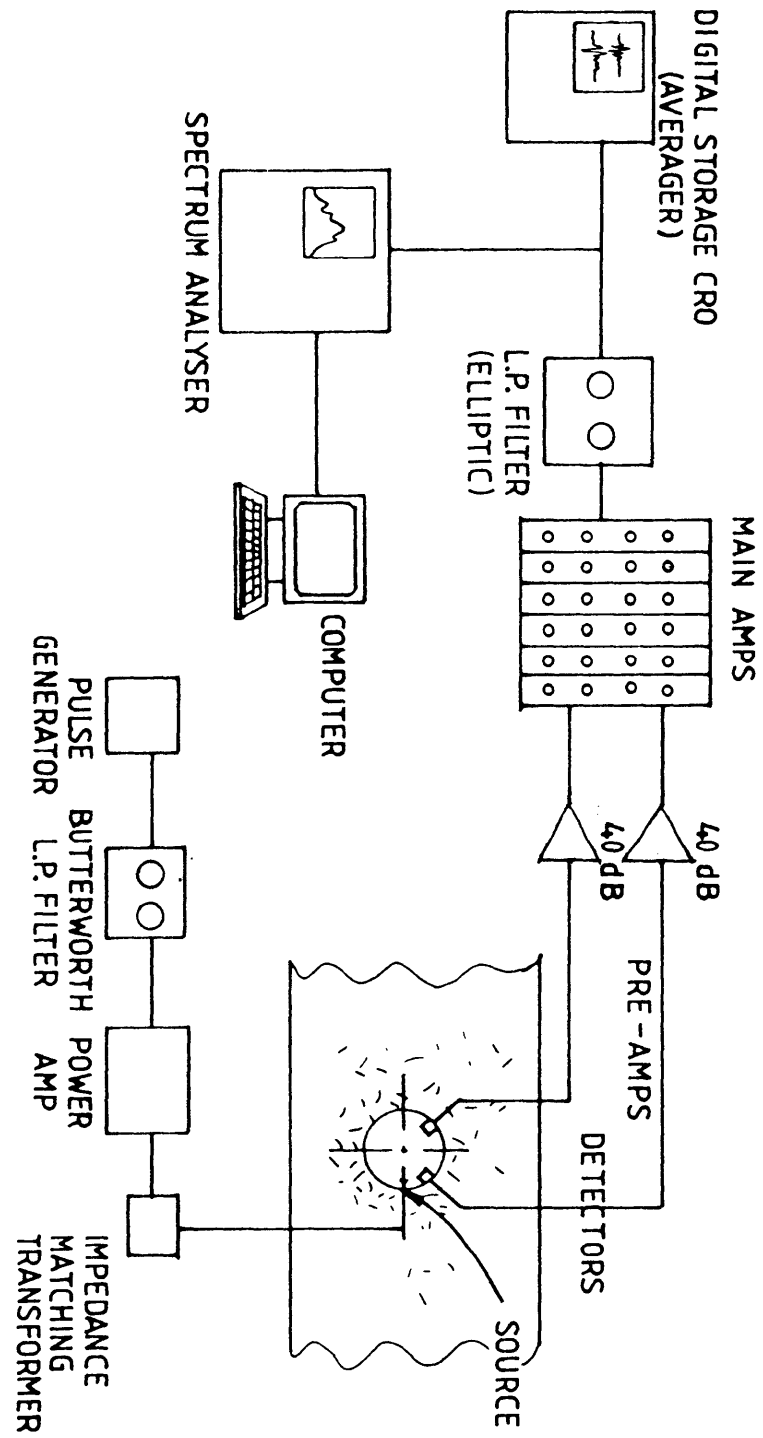

Figure 30. A schematic diagram of the instrumentation of the bore-hole.

Titanate (PZT-4). Parallel lines, approximately 3mm apart, were scored on a silvered disc surface. Pressure was applied, breaking the disc along the scored lines. The resulting strips were then lapped on a diamond impregnated lapping table, ultimately producing suitably shaped elements for placement on the borehole wall parallel to the borehole axis. Some of these piezo-electric elements are illustrated in Figure 31.

Miniature accelerometers, Bruel and Kjaer types 4344 and 4374, were used as detectors. Detector accelerometers were coupled to the rock using beeswax (The applicability of beeswax as a coupling agent is discussed in Bruel and Kjaer, 1974, BR0173).

A piezo-electric element (of similar form to those described above) was cemented with polyester resin to the borehole wall at 0^{o} with its long axis parallel to the borehole axis. The source and detector configuration within the borehole is illustrated in Figure 29(b). A reference accelerometer was placed at 10^{o} from the source. All timing measurements were made with respect to this reference accelerometer.

7.2.1 Experimental procedure

A pulsed excitation voltage in the form of a positive going pulse of 5 milliseconds width was applied to the piezo-electric element. Waveforms were recorded at 30 degree intervals around the test cross-section. Waveform durations were of the order of 2 milliseconds. Initial experiments with this form of excitation yielded waveforms with a dominant frequency component of 100 kHz. This frequency corresponds closely to the mounted resonance of the accelerometers used (Bruel and Kjaer type 4344). This suggested that the rapid rise-time of the applied "high" voltage pulse excited unwanted resonance in the accelerometers. Consequently a filtered pulse was applied to the piezo-electric element. This pulse was obtained by decreasing the rise-time of the applied voltage via the signal generator.

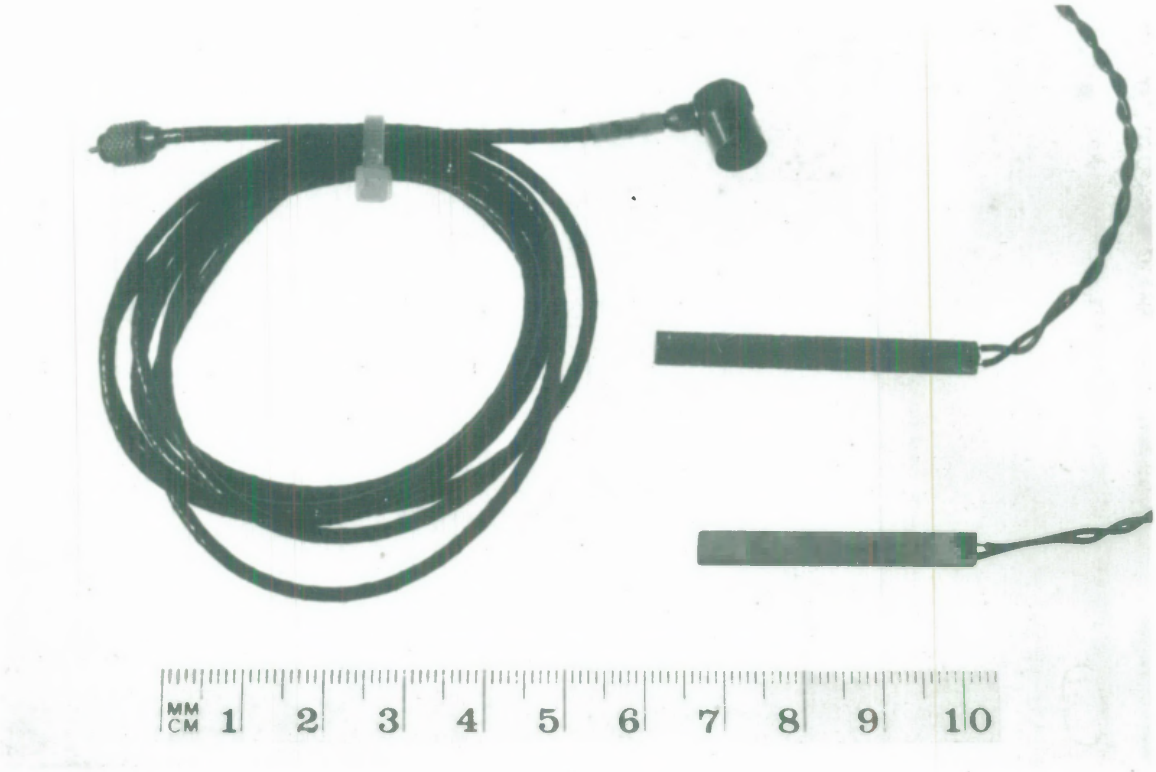

(a)

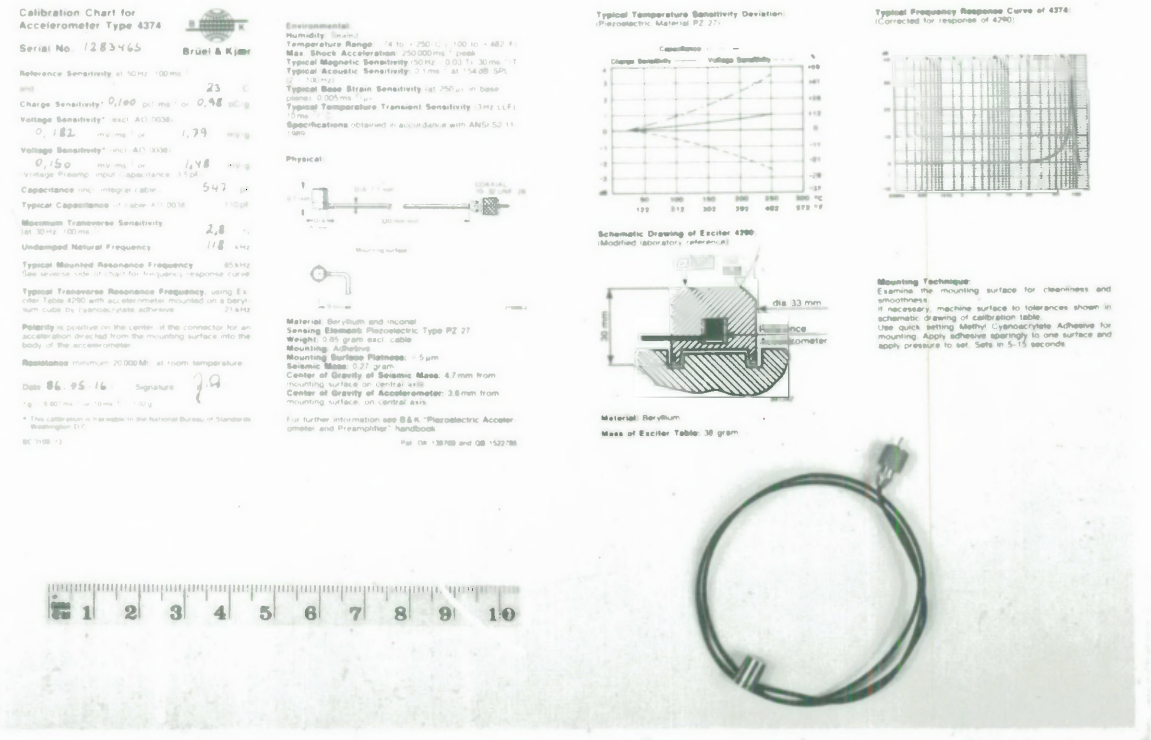

(b)

Figure 31 (a). Piezo-electric source elements used for excitation of test cross-sections in the bore-hole together with an accelerometer B &K type 4344, (b) accelerometers B&K type 4374 used for the majority of the experimental work

Detected waveforms around the test cross -section were then found to be independent of detector type, i.e., when 4374 type accelerometers were substituted for 4334 types no change in observed waveforms was apparent. With the use of a Nicolet 1170 averaging digital oscilloscope, waveforms at each detector location were averaged (128 averages per waveform). Waveforms were recorded with the digital storage oscilloscope operating in transient-capture mode with pre-trigger set to a constant value; thus, it should be noted that zero (0) on the waveform plots has no significance - all timing measurements were made with respect to a reference accelerometer at -10°.

Attention was then directed to the waveform at each detector position. It was noticed that a relatively high amplitude pulse appeared in all waveforms at approximately 350 microseconds. This was puzzling at first since care had been taken to check all possible sources of reflection. Waveforms had been monitored on all possible reflecting surfaces (i.e., at adjacent holes and free surfaces of the block) with the use of a roving accelerometer. Amplitudes at these surfaces were found to be typically 40db down from signals measured in the test cross-section. Thus, when re-radiation (with further geometric spreading losses) and further attenuation is considered as the reflected pulse returns to the test cross-section its contribution will be negligible.

However, it was soon realised that one possible path had not been considered, i.e., that of a guided "Rayleigh" wave travelling down the borehole wall, parallel to the borehole axis. This wave is then reflected at the borehole boundary at the free surface of the block and returns to the test cross-section as a pulse with comparable amplitude to that of the circulating energy.

The measured arrival time of 350 microseconds agrees closely with the time taken for a wave travelling at 2580 m/s to traverse the 0.9m from the central cross-section to the edge of the borehole and back.

7.2.2 Circulating waves on a test section at the end of the borehole

In an attempt to compensate for the finite length of the borehole a new test cross-section was selected at the end of the central borehole. The excitation voltage pulse supplied to the piezo-electric element was of the form of the impulse response of a low-pass, 4th-order, Butterworth filter (obtained with a Kronhite Model 3550 filter), with the 3db point set to 20 kHz. The measured waveforms were filtered with a low pass elliptic filter (Precision Filters, Model 602) with the 3db point set to 30kHz.

This means that the circulating pulse should complete nearly three circuits of the cavity (one circuit takes approximately 240 microseconds measured using first peak arrivals) before it is contaminated by the reflection from the borehole-end returning at an expected time of 670 microseconds.

7.3 Results and discussion

Circumferential transit times were calculated from the first breaks, the 10% and 90% amplitude levels of the first peak, and the first peak maxima. An average velocity of 2653m/s was arrived at using the first break of the circulating waveforms as a time-pick. (When this velocity is regarded as the Rayleigh wave velocity and used in conjunction with the experimentally determined compressional wave velocity of 4690 m/s, a Poisson's ratio of 0.19 is obtained which is in close agreement with Poisson's ratio deduced from the compressional and shear velocities.)

Figure 32 presents waveforms recorded at 30 degree intervals around the test cross-section at the borehole end. Waveforms can be seen to consist of a primary pulse consisting of approximately 6 oscillations with an approximate period of 37 microseconds. The duration of this packet is approximately 240 microseconds. This is

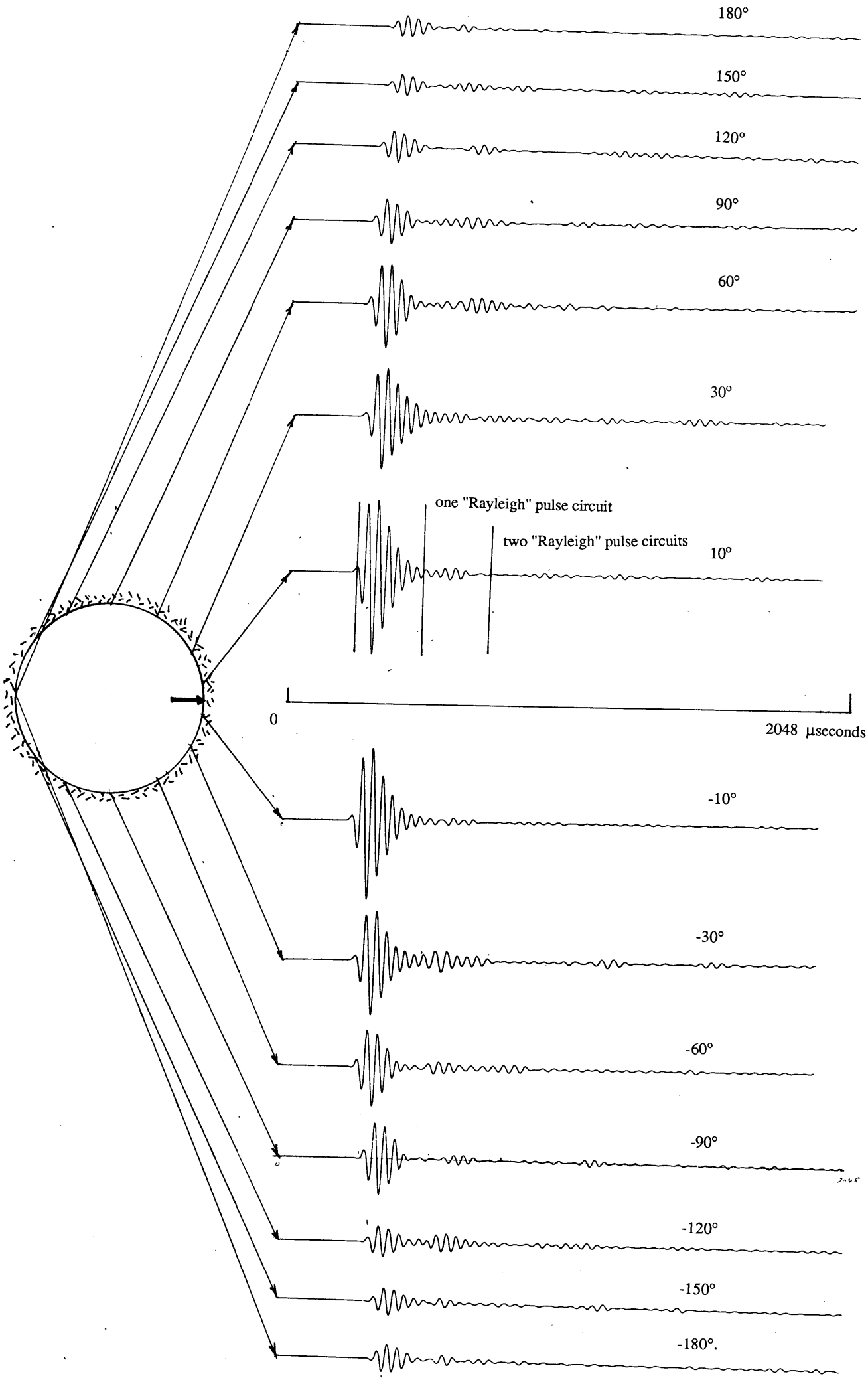

Figure 32. Waveforms recorded at intervals around the test cross-section (gains varied from 63 dB at 10° to 87dB at 180°).

followed by a lower amplitude packet of a similar number of oscillations and of similar time-duration. However, the approximate period of the oscillations is now 40 microseconds. This is interpreted as the second circuit of the circulating pulse. Dispersive propagation, resulting from a combination of bore-hole geometry effects and frequency dependent attenuation, has reduced the frequency content of this circulating energy.

An approximation to the source acceleration spectrum was measured by mounting a miniature accelerometer (Bruel and Kjaer type 4374) on to the back of the piezo-electric element and recording the resulting spectrum with the use of a Rocklands 512 spectrum analyser. This spectrum is presented in Figure 33 together with the time-domain waveform and electrical pulse supplied to the source element. Similarities between this spectrum and the source pulse used in both DFEM studies and the analytical calculations are apparent. This facilitates comparisons between experimental and theoretical waveforms. Figure 34 presents theoretical, circumferential, travel-time curves obtained from the DFEM results together with experimental results plotted against dimensionless time, $tC_D/2a$. The time pick used in both cases was the first peak maxima.

As can be seen from these results the travel-time curves have several branches - this is due to the change in sign of the first peak as the pulse progresses around the cavity in both the experiment and DFEM model. For example, assume the first peak is positive, as θ increases, this peak will increase in amplitude until the appearance of as new negative peak. This peak, in turn, increases in amplitude until a new positive peak is observed. Each individual curve is obtained from tracking the maximum of a peak of constant sign. The slope of the theoretical curves and best fit to the experimental curves is $0.44C_D$.

The progressive changes of sign as the waveform packet circulates is direct evidence of the dispersive nature of the propagation. These changes in the waveform are directly related to the radiation of bulk wave modes (shear and longitudinal) into the

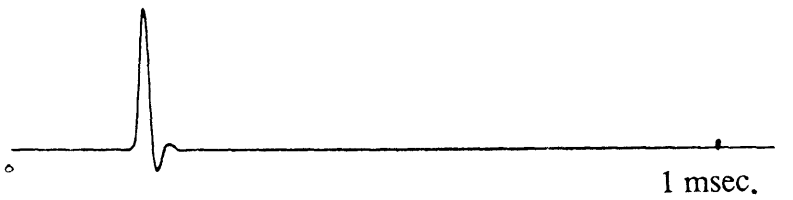

(a) electrical pulse supplied to piezo-electric source.

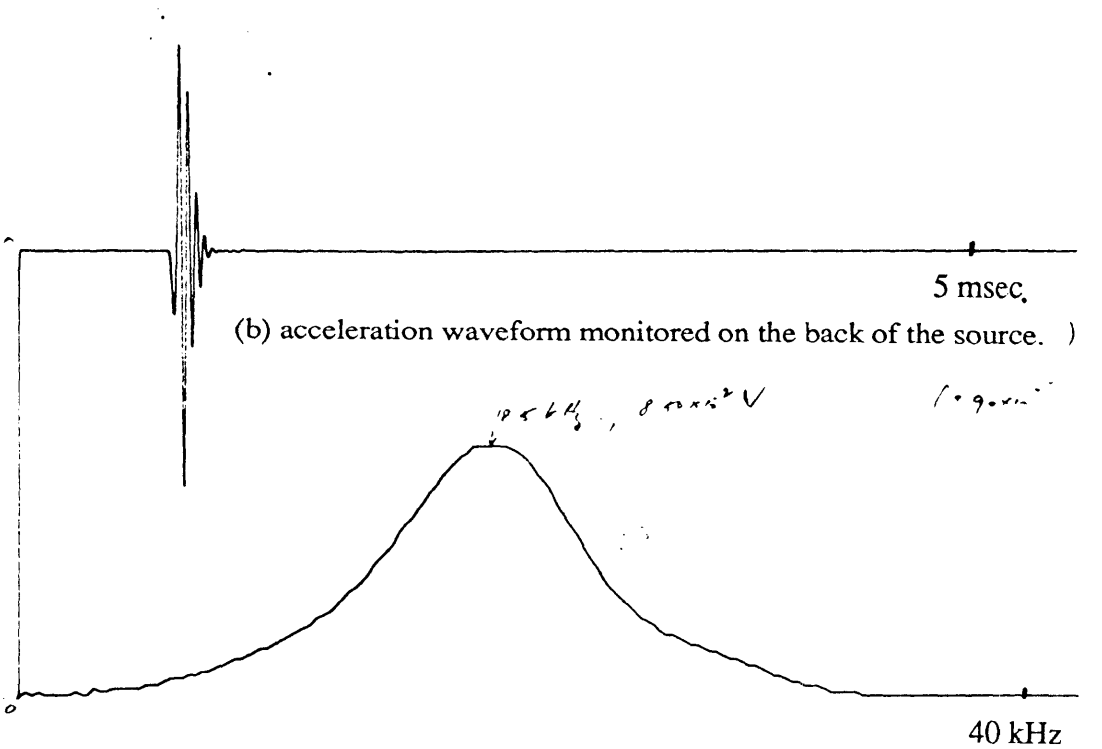

(c) spectral response of the source.

Figure 33. Input pulse and corresponding spectrum monitored on the back of the piezo-electric source. This spectrum was used for all spectral ratio calculations.

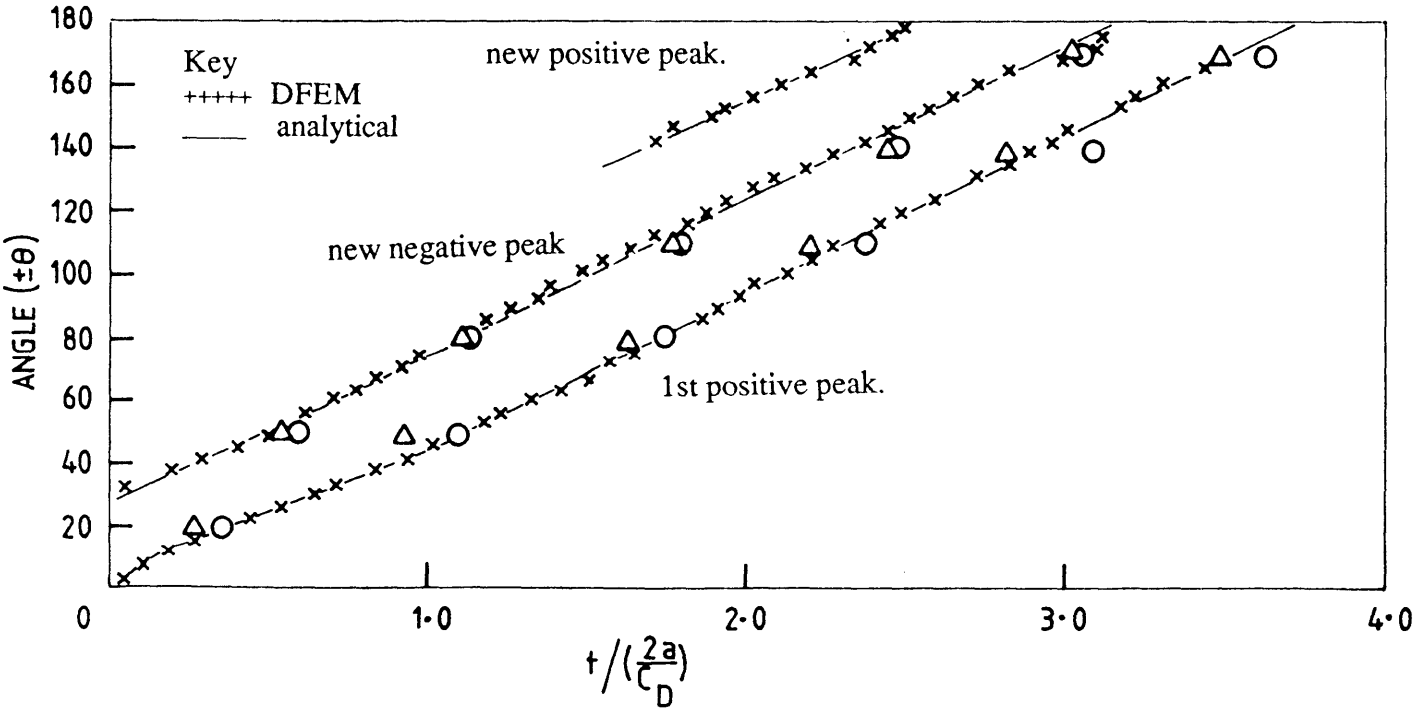

Figure 34. Travel times of circulating pulses around the test cross-section.

Experiment: o indicates travel times on the upper half of the bore-hole

Δ " lower "

surrounding medium and are most probably accompanied by the presence of "shooting tips" as observed by Ying et al (1981).

When comparing the total waveforms around the test cross section there is a noticeable lack of symmetry between waveforms recorded at the equivalent positions on either side of the plane of symmetry, see Figure 32. In particular, there is a measurable velocity discrepancy of the order of 83 microseconds (when plotting first peak positions) between top and bottom halves of the borehole, see Figure 34, despite the apparent uniformity of the rock texture. This may result in constructive and destructive interference between pulses travelling in opposite directions.

One possible explanation for the velocity discrepancy that requires examination is that of stress-velocity effects. At first sight this possibility is supported by the fact that pulse arrival times are generally shorter on the lower half of the borehole when compared to arrival times at corresponding points on the upper half. However, this implies that the velocity of the "Rayleigh" waves is higher on the side of the bore-hole under static tensile stresses than that under static compressive stress (the stress differential between upper and lower halves of the borehole, due to the weight of the block, can be calculated from simple beam theory - allowing for stress concentration at the borehole boundaries, to be of the order of 0.2MPa). This is at variance with the results of experiments designed to measure stress-induced elastic wave velocity-anisotropy reported by several authors including, Gladwin and Stacey (1974), Blair, Siggins and Wold (1984) and Su et al. (1983) who reported negative velocity-stress sensitivities. In addition, the apparent stress velocity sensitivity, $\Delta v/v$ per MPa, of 20%/MPa is twice as great as the highest sensitivity yet reported (by Su et al., 1983 who obtained for sandstone samples a stress velocity sensitivity of the order of -10%/MPa).

A more likely explanation is the presence of subtle variations in the Harcourt granite texture resulting in small scale heterogeneous velocity distributions throughout the block.

In fact, pulse attenuation experiments conducted by Dr. Blair (personal communication, 1987) on the block suggest that aggregations of grains within the rock can function as scattering centres despite the small grain size of the granite with respect to seismic wavelength. Thus, these aggregations will have acoustic impedance contrasts to the average properties and hence velocity differences.

These heterogeneities, if they do exist, would be expected to be more clearly revealed in the frequency domain since pulse reflections from such regions would result in substantial complexity and asymmetry in the spectral response when comparing corresponding points on both halves of the borehole test cross section. Figure 35(a) illustrates the spectral ratio (output acceleration/input acceleration) response of the test cross-section. As can be seen the spectral ratio behaviour is somewhat more complicated than that expected from the theoretical models and some asymmetry is present. There is also a peak present at 1.5 kHz in spectra recorded close to the origin. This corresponds to the time delay of 670 microseconds associated with the "Rayleigh "wave propagating along the borehole axis, reflecting from the free surface of the block, and returning to the test cross-section. The experimental spectral acceleration-ratio curves are not strictly comparable in shape to the corresponding theoretical plots since the latter curves are displacement/stress ratios.

The borehole "modal" behaviour is plotted in Figure 35(b) for the dominant peak at 38.8 ± 0.3 kHz. This peak corresponds to a wavenumber k_1a of 3.95 which is the 9th normal-mode for a cavity in an infinite elastic medium with a Poisson's ratio of 0.2. The 9th normal mode is associated with 8 oscillations in the transfer functions since the normal modes on the Rayleigh branch begin at n = 2. An examination of the experimental transfer function curves show that, on average, this peak corresponds to the 8th major oscillation.

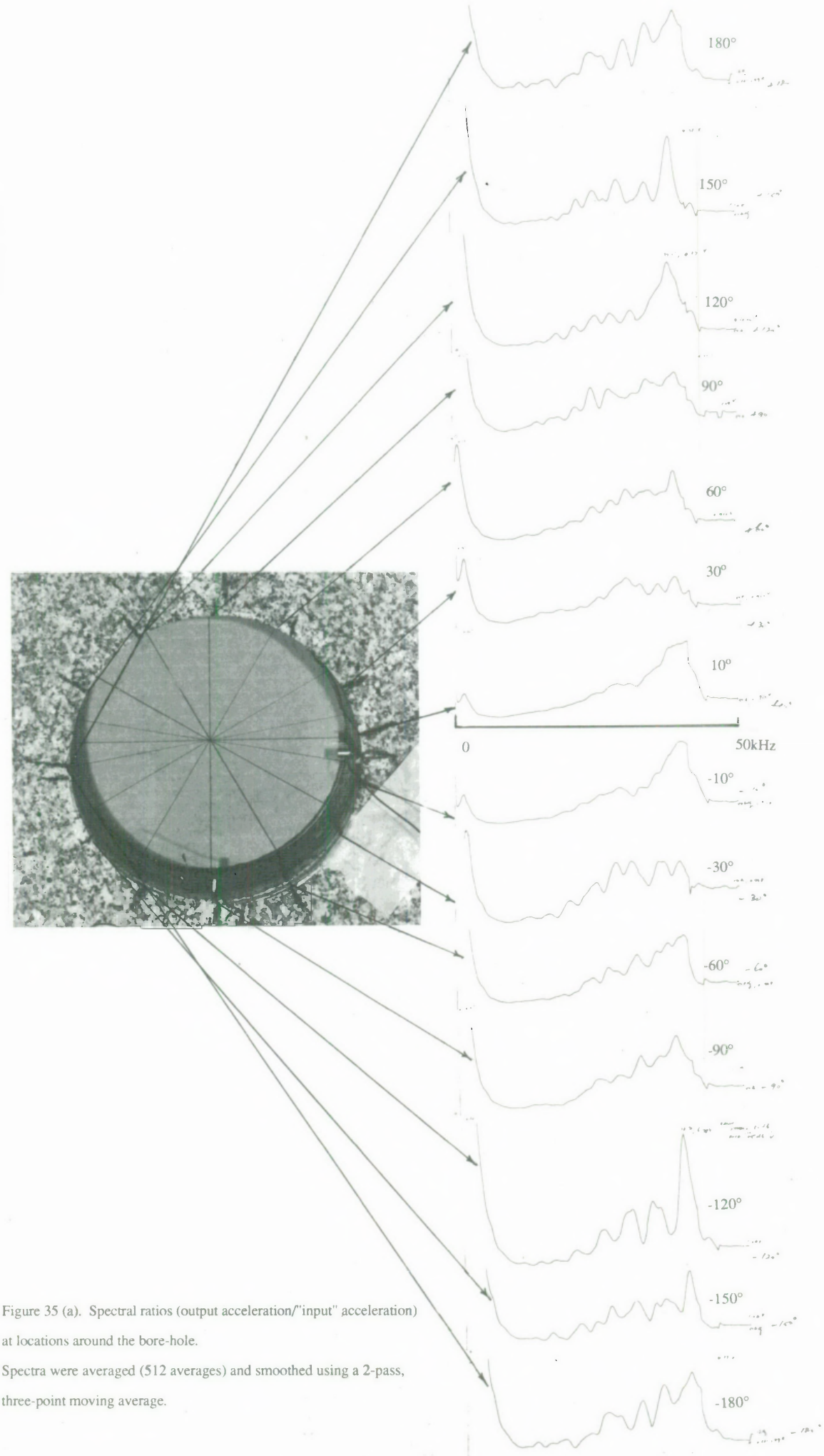

Figure 35 (a). Spectral ratios (output acceleration/"input" acceleration) at locations around the bore-hole.

Spectra were averaged (512 averages) and smoothed using a 2-pass, three-point moving average.

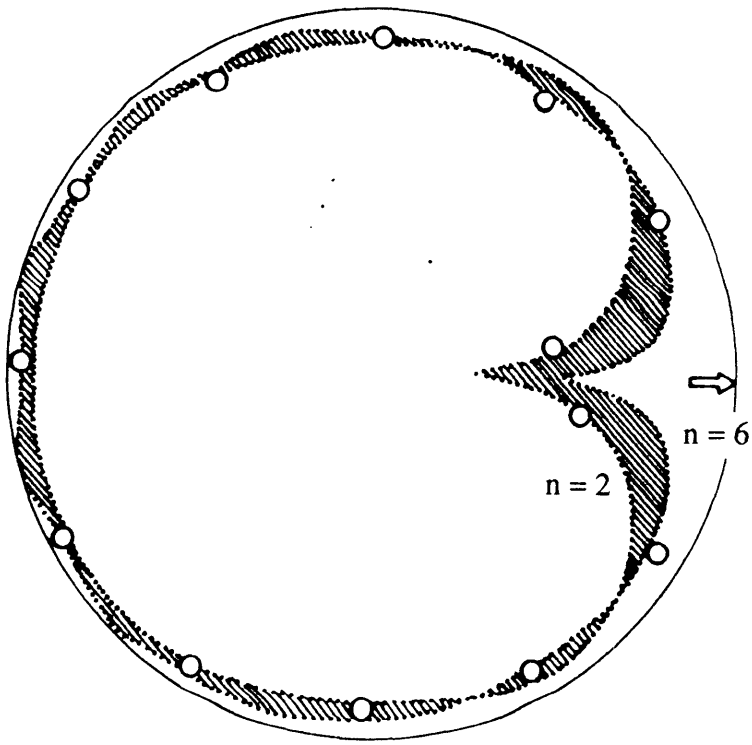

Figure 35 (b). Borehole modal behaviour at 38.8 kHz corresponding to $k_1a = 3.95$. Experimental points, indicated by **o**, are superimposed on theoretical modes 2 to 6.

8. Observations of circulating elastic waves in the field

The initial site selected for experiments on circulating elastic waves was in a blind heading on the 17th level, Southern B Lode, New Broken Hill Corporation Mine, Broken Hill, New South Wales. The heading had been constructed using drill and blast techniques. Production was in progress in an adjacent stope. The rock at this site was classified as a Gneiss with Pegmatite intrusions. Additional sites were tested at the Geophysical Observatory tunnel, Hillgrove, Armidale, N.S.W.

8.1 Laboratory measurements of rock mechanical properties

Prior to the field experiments at Broken Hill, cores were taken from diamond drilled boreholes at the site and prepared for laboratory testing. Elastic moduli of the four cores prepared were measured with both static and dynamic techniques. Figure 36 illustrates the instrumented cores together with the piezo-electric elements used for resonance testing of the cores.

The static compression tests were carried out in accordance with the International Society for Rock Mechanics (ISRM) recommendations. In these tests the ends of the cores are lapped parallel to fine tolerances (±0.02mm). Strain gauge rosettes are then cemented to the central portion of the cores This enables both axial and circumferential strains to be measured as a function of compressive stress applied via a testing machine. Results are processed to yield Young's modulus, E, shear modulus, μ, and Poisson's ratio, ν.

The corresponding dynamic elastic constants were determined by measurements of longitudinal and torsional vibrational resonances. These tests were carried out in accordance with the ISRM Recommended Methods, Dynamic Elastic Tests (currently under revision by the author). Testing involves attaching piezo-electric source elements -

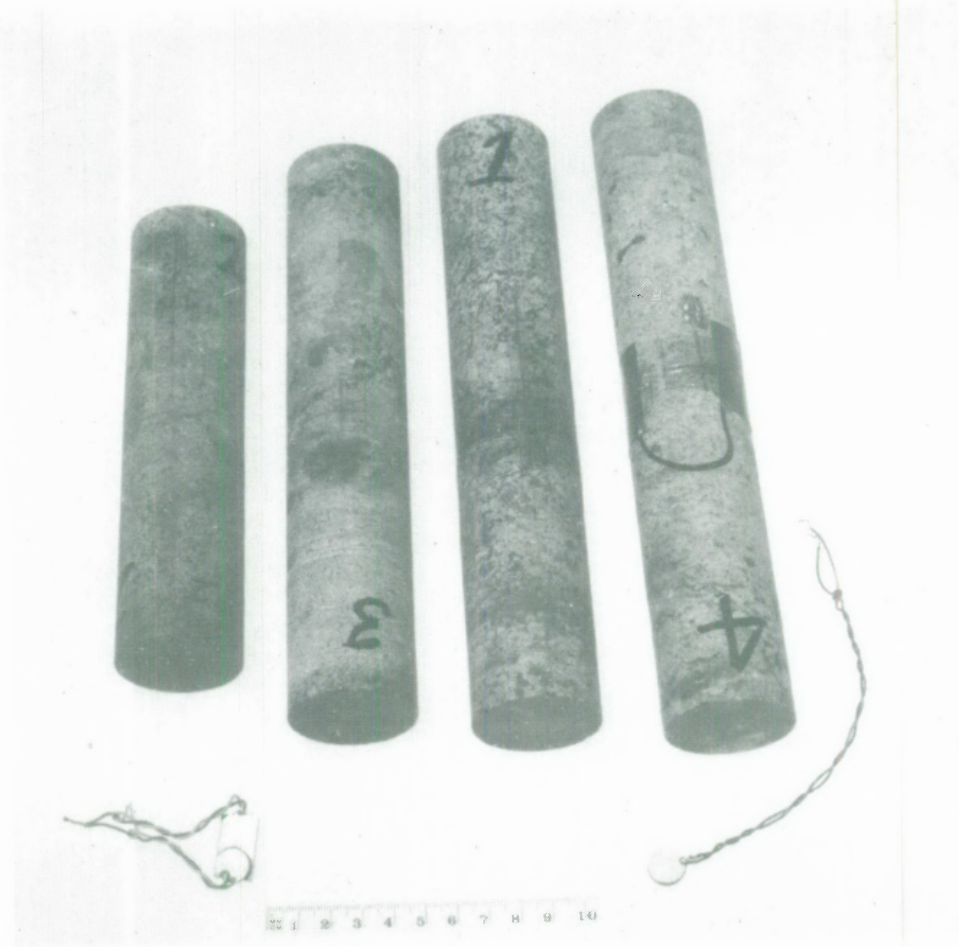

Figure 36. Strain gauged rock cores from diamond drilled bore-holes at the Broken Hill test site together with piezo-electric elements for dynamic resonance tests. The device on the left is torsional source whereas that on the right is a longitudinal source.

shown in Figure 36, to the lapped ends of the cores. Miniature accelerometers were attached to the opposite ends of the cores. (The piezo-electric torsional source was developed specifically for these tests). The cores were then suspended by nylon filaments attached to the mid-point of the cores. Fundamental resonance frequencies, both torsional and longitudinal, were measured by applying a swept sinusoidal signal to the piezo-electric source and monitoring the amplified accelerometer output with the use of a Rocklands 512 Spectrum analyser. Resonance is manifested by a rapid increase in signal output with an accompanying 180 degrees phase transition between input and output signals. Dynamic moduli can then be calculated from these resonances using standard formulae, see Siggins (1986) for example.

Table 5 provides a comparison between static and dynamic moduli determined in these tests.

Core No.	DYNAMIC (resonance)			STATIC (compression)		
	E(GPa)	μ(GPa)	ν*	E(GPa)	μ(GPa)	ν
1	74.1	33.6	0.10	76.7	32.1	0.20
2	58.1	34.2	--	82.1	37.9	0.08
3	45.4	26.1	--	63.2	26.0	0.22
4	47.4	23.6	0.01	44.7	19.7	0.13
Average	56.3	29.4	0.06	66.7	28.9	0.16
Std. dev.	13.1	5.3	--	16.7	7.8	0.06

*The calculation of Poisson's ratio from the dynamic moduli is inaccurate and particularly unstable when E approaches 2μ.

8.2 Instrumentation of the field site

The selected test section of the drive was prepared by first removing all loose rock. Thirty five holes of 15mm diameter were then bored in radial directions at approximately

six degree intervals around the accessible portion of the test cross-section (approx. 220 degrees). Knurled stainless steel pins (13mm diameter and 75mm in length) were then grouted into each bore-hole using a two-part polyester resin (Plasti-bond). These pins had been previously drilled and tapped to accept the mounting stud of a Bruel and Kjaer type 4334 accelerometer, refer to Figure 37(a). The accelerometer locations at the test site are illustrated in Figure 37(b).

The seismic source employed for these experiments consisted of a 300 watt electro-mechanical shaker, Ling Model No. 402 - Figure 38 (a). Instrumentation to drive the shaker and record waveforms at points in the accelerometer array is illustrated in Figure 38(b). A schematic diagram of the equipment is presented in Figure 39.

Mounting of the shaker to the drive-way roof was performed in the following manner: A 6mm thick steel plate was installed at the approximate centre of the roof. This was accomplished by bonding the plate to the roof with the polyester resin. Four 10mm holes were then bored into the roof material through the existing holes in the plate. Expanding bolts (Loxins) were then placed in these holes and tightened. The tightened bolts provided an adequate clamping force. However, this was supplemented by the resin bond which helped to ensure that no spurious resonances in the dynamic behaviour of the source would be introduced via the mounting.

A heavy duty piezo-electric dynamic force gauge was then bolted to the plate and the shaker unit bolted to the force gauge in turn. The force gauge allowed the input force spectrum to be measured at the point of application. This device, illustrated in Figures 40 and 41, was developed specifically for these experiments and is the subject of a provisional patent. (A copy of the covering letter concerning patent approval is included in Appendix 2). Figure 42 presents details of the shaker and mounting arrangement. A 15 kg brass disc, attached to the shaker armature, can be seen in the illustration; the

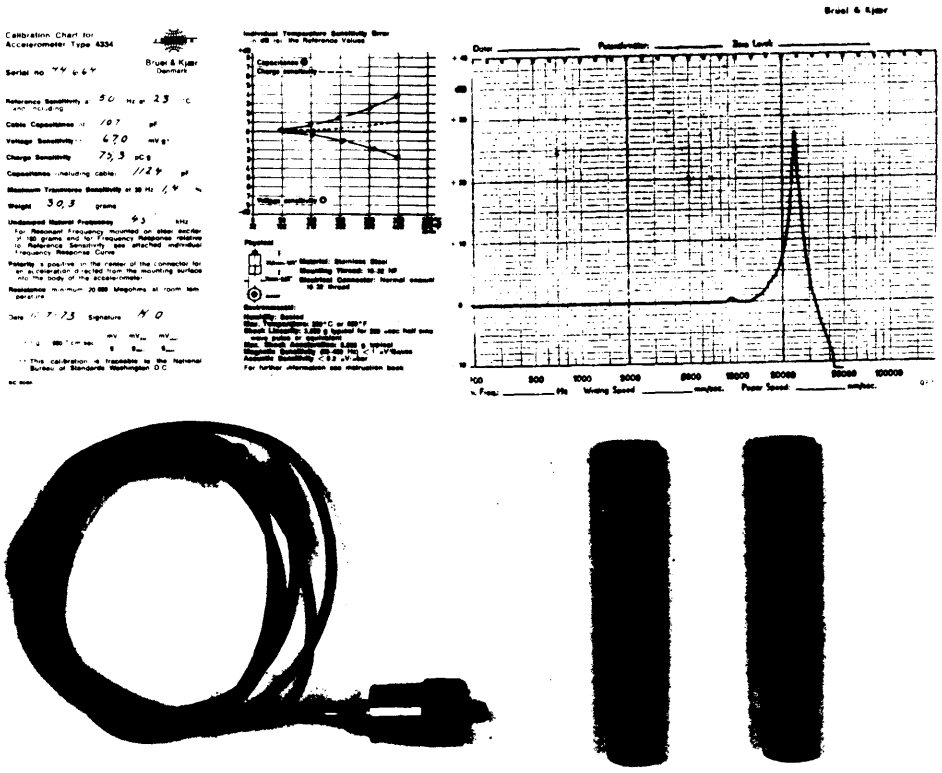

(a)

(b)

Figure 37 (a). Accelerometers (type B&K 4334) and mounting pins; (b) accelerometer locations at the test cross-section.

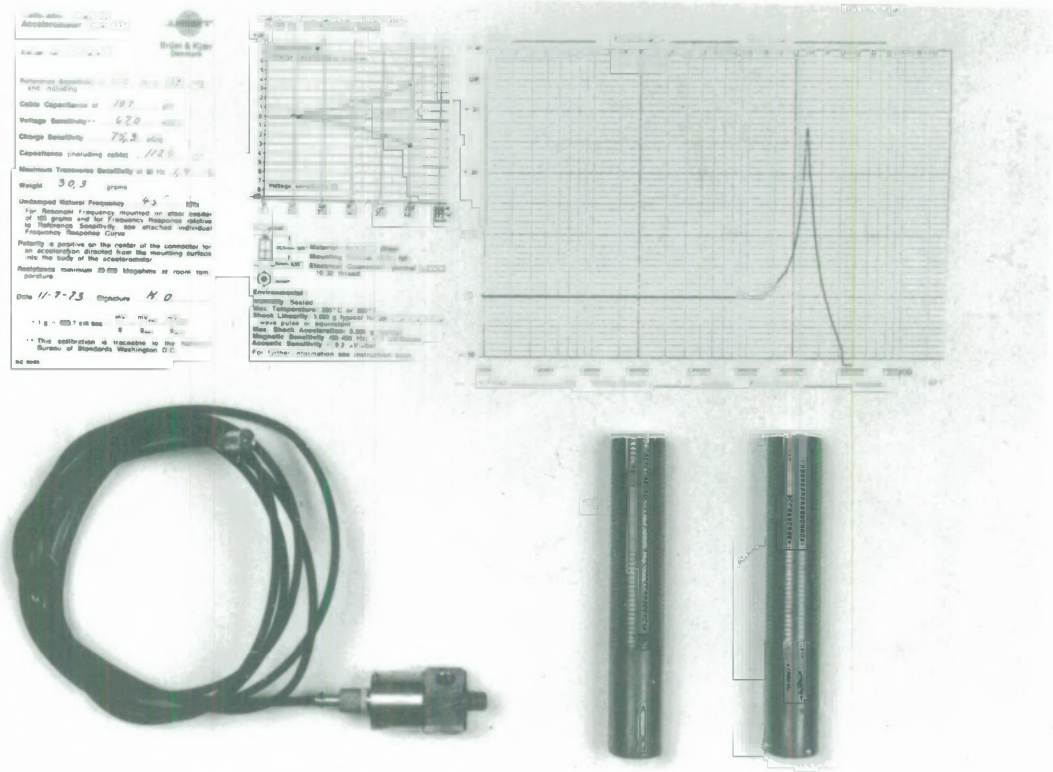

(a)

(b)

Figure 37 (a). Accelerometers (type B&K 4334) and mounting pins; (b) accelerometer locations at the test cross-section

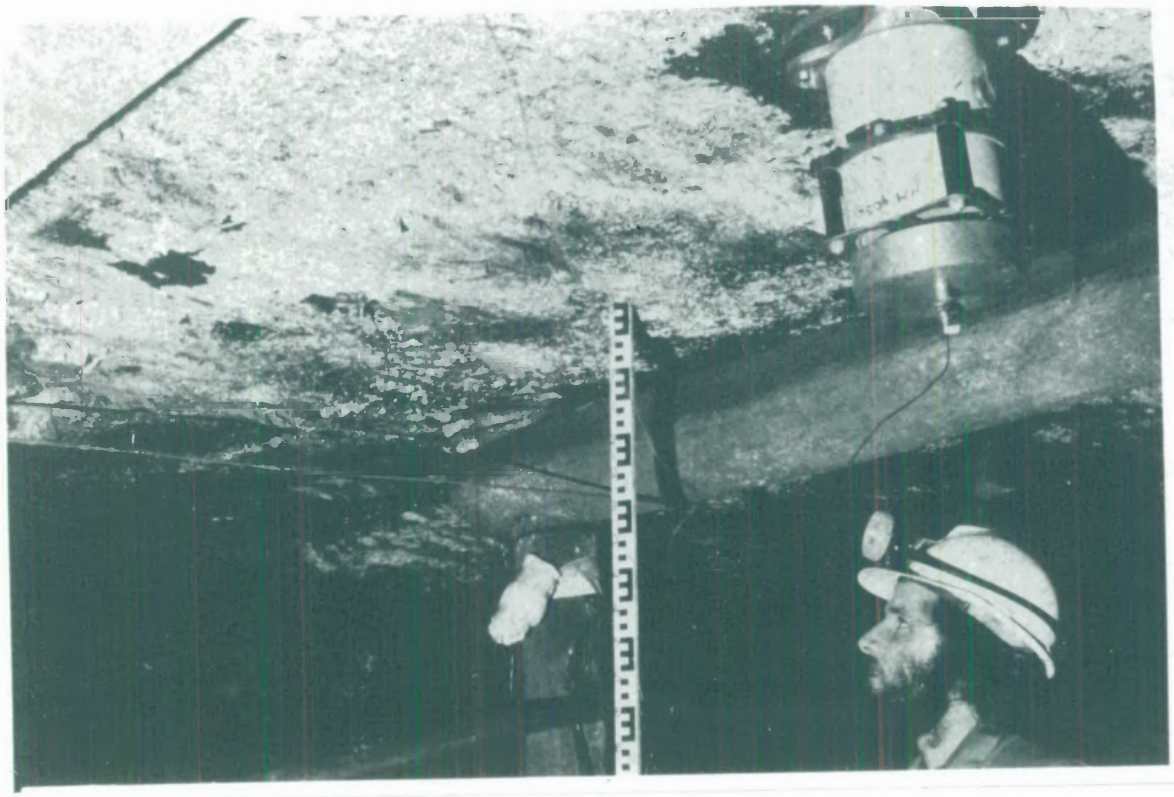

(a)

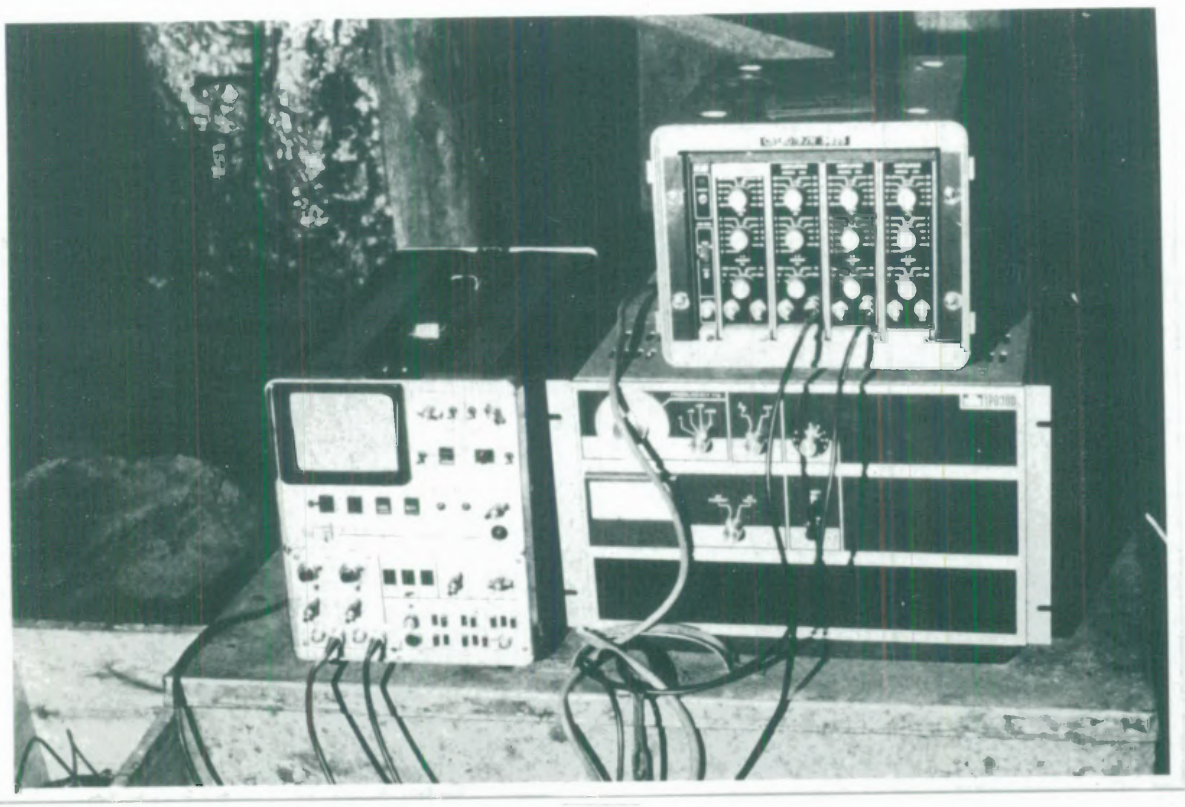

(b)

Figure 38. Shaker source in position (in this case attached to the roof of a coal mine heading). (b) Instrumentation used at the Broken Hill test site consisting of power amplifier, signal amplifier bank and oscilloscope. The spectrum analyser and tape recorder are out of the picture.

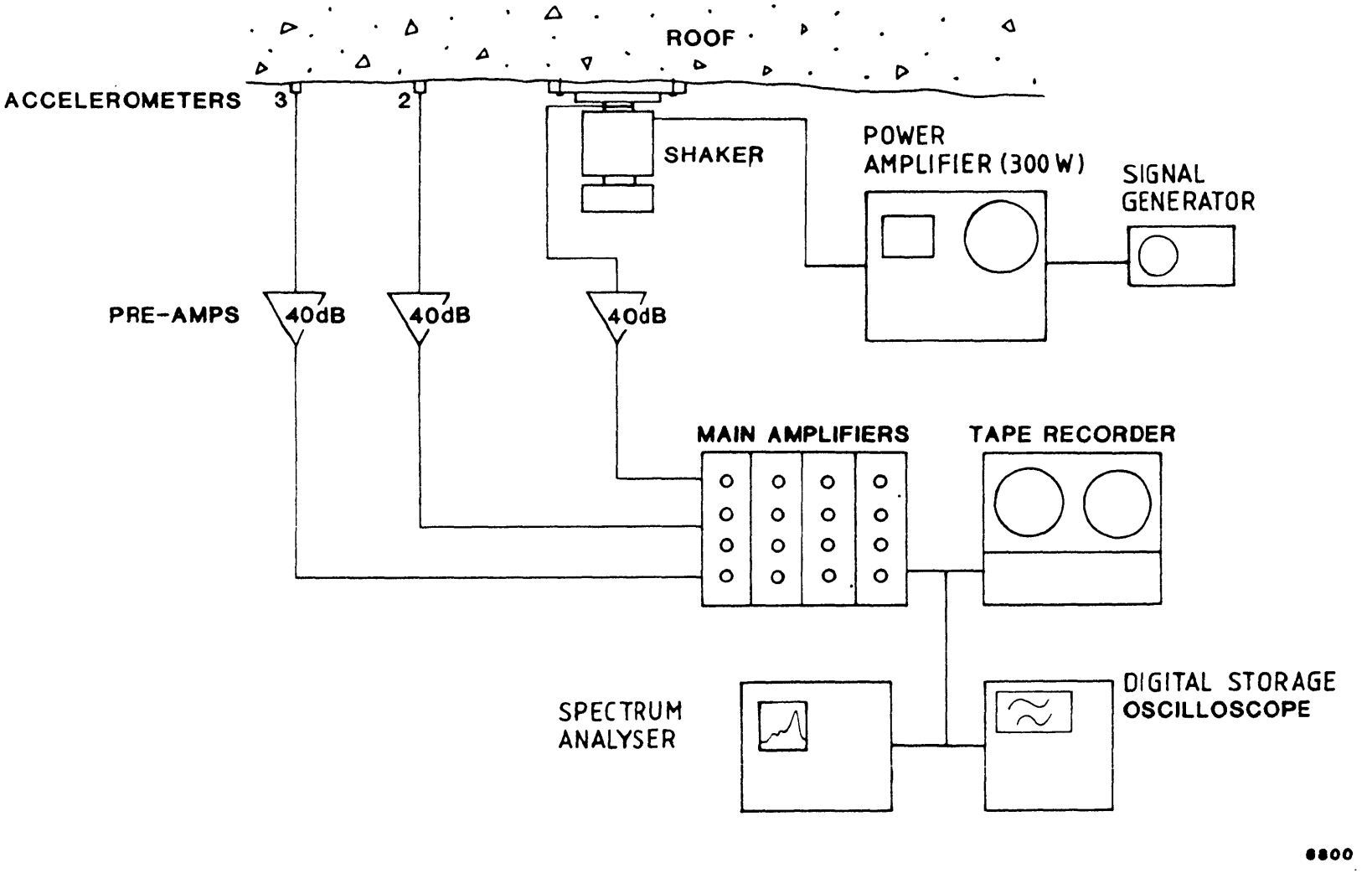

Figure 39. Schematic of instrumentation.

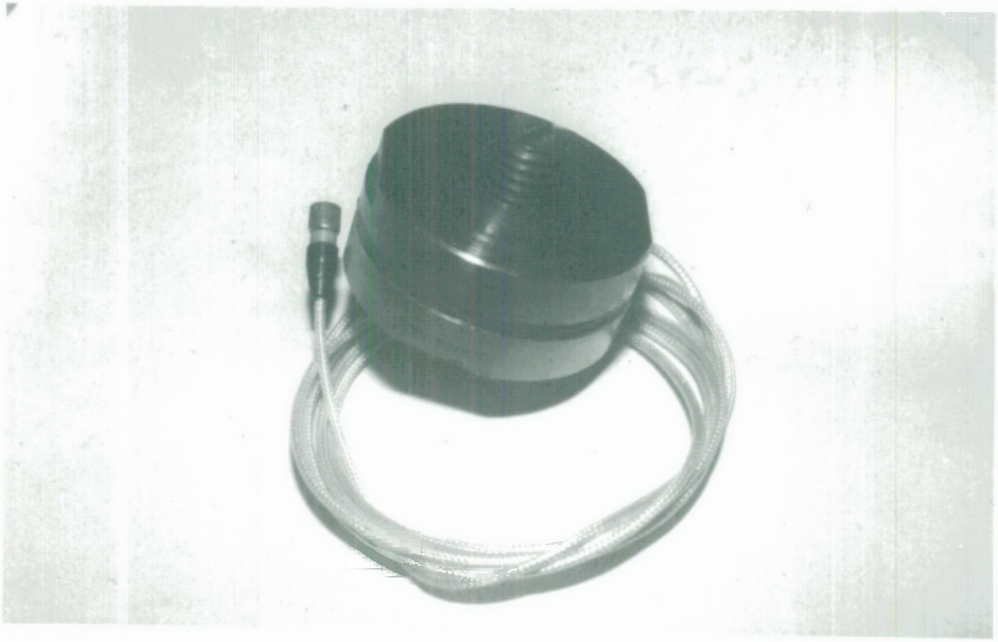

Figure 40. Force gauge developed for mine-opening resonance testing.

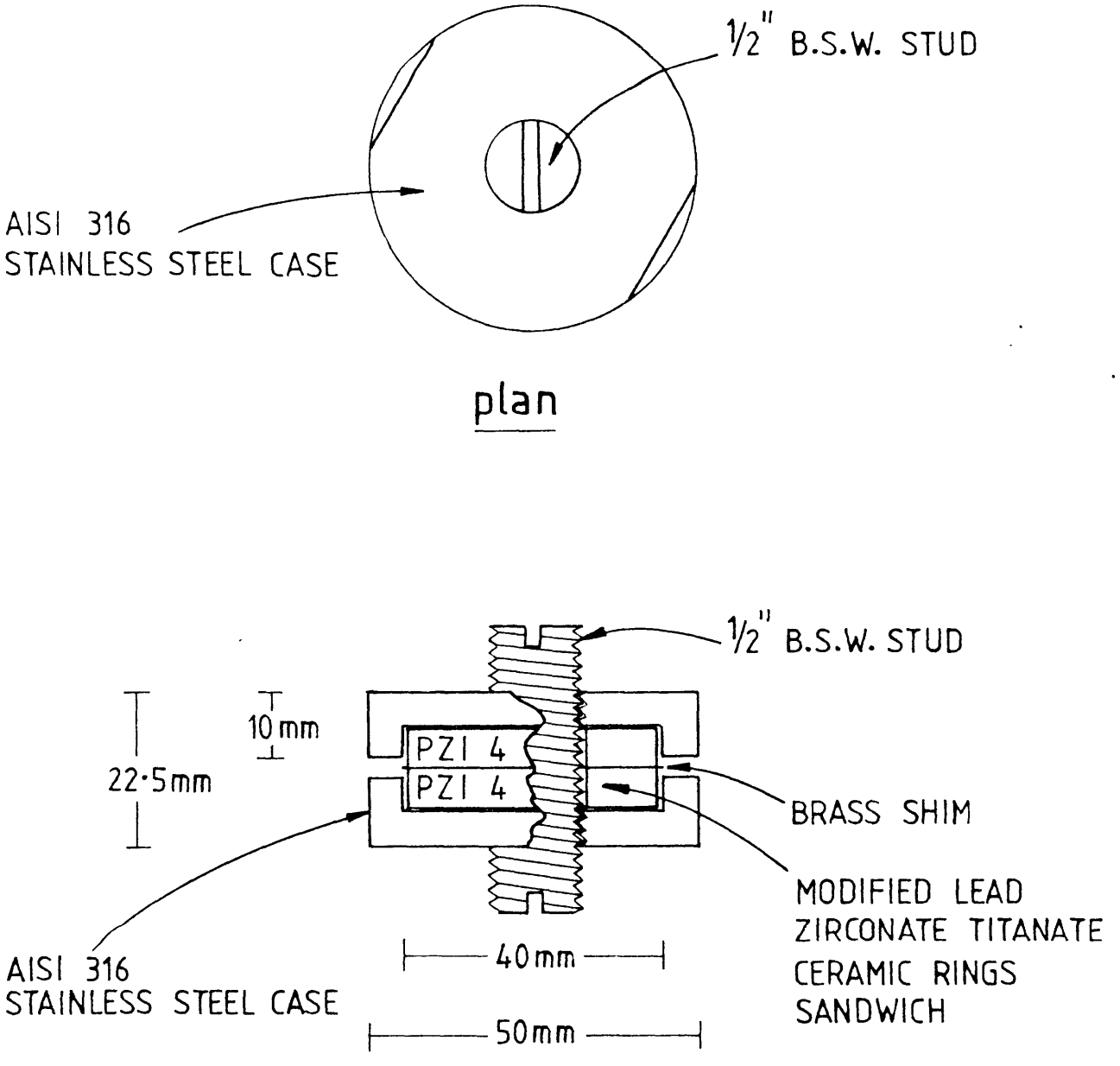

Figure 41. Sectioned view of force gauge construction.

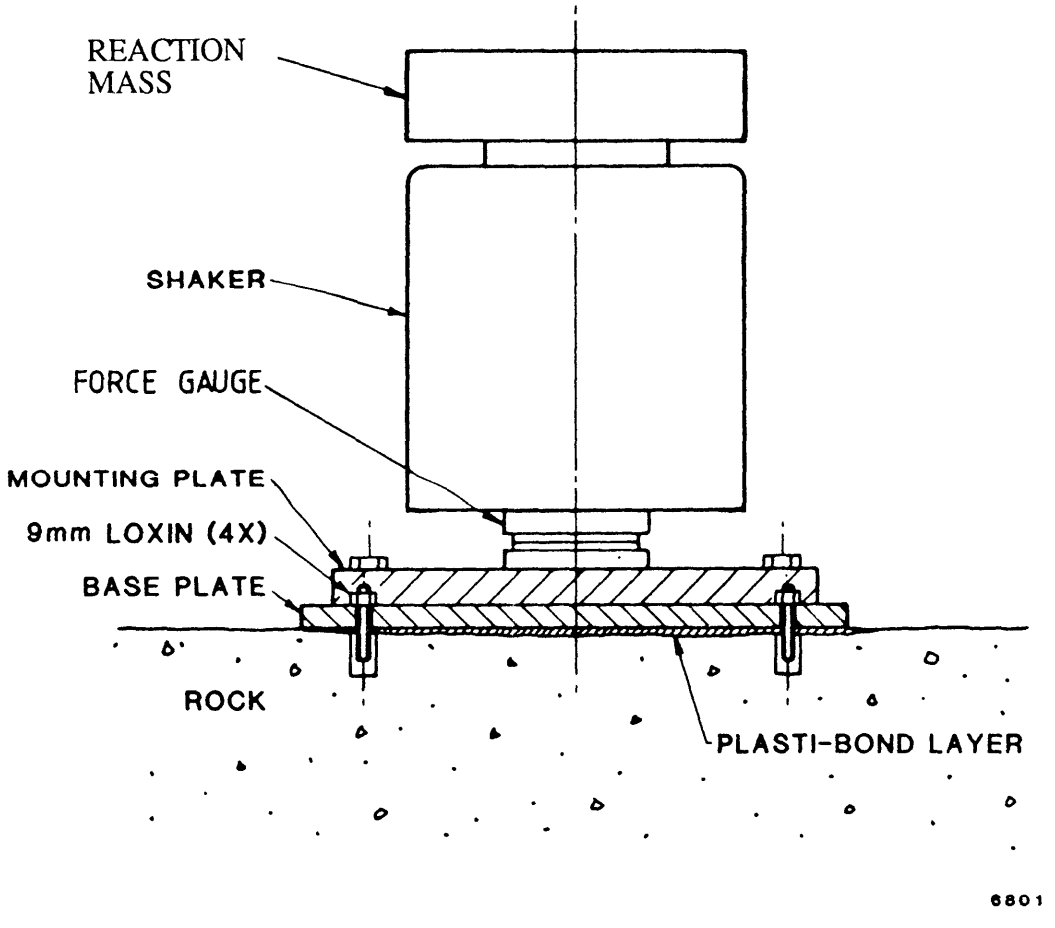

Figure 42. Details of shaker mounting arrangement.

additional mass functioned as a reaction mass to improve the seismic coupling into the rock.

When sufficient time had elapsed for the resin to fully cure, accelerometers (Bruel and Kjaer type 4334) were attached to the mounting pins. (To ensure repeatability each accelerometer was attached using a pre-determined mounting torque of 10Nm measured via a small torque wrench.) The power oscillator driving the shaker source was then swept from 20 Hz to 2 kHz over a period of approximately 10 minutes providing a sinusoidal signal varying slowly in frequency, but with constant amplitude. A sweep down from 2 kHz to 20 Hz was carried out in a similar manner. This process was repeated for all accelerometer locations in the array. This testing procedure, termed the swept-sine method, is a particularly accurate means of measuring resonant frequencies.

The force gauge output and accelerometer responses at locations around the test cross-section were recorded on magnetic tape and concurrently with the use of a spectrum analyser. Plots of spectral ratios between input force and output acceleration were obtained with the use of an X-Y plotter connected to the spectrum analyser. Some difficulty was experienced with mining noise contamination and poor condition of the rock around the test cross section; however, data were recorded, in the main, during quiet conditions and repeatability was checked over a period of several days.

8.3 Results and discussion.

The spectral response of the test cross-section in the form of output acceleration divided by input force at the accelerometer points (only 16 points were eventually considered competent) is presented in Figure 43. As can be seen, the spectral behaviour at the majority of points in the array can be summarised as consisting of a dominant peak at 1750 Hz accompanied by two smaller peaks at 1200 Hz and 1480Hz. The input force

Figure 43. Dynamic response of test cross-section. Spectral ratio plots (output acceleration/ input force) are presented at various locations around the test cross-section. Gains varied from 70 dB, location 19, (adjacent to source) to 100dB at location 32.

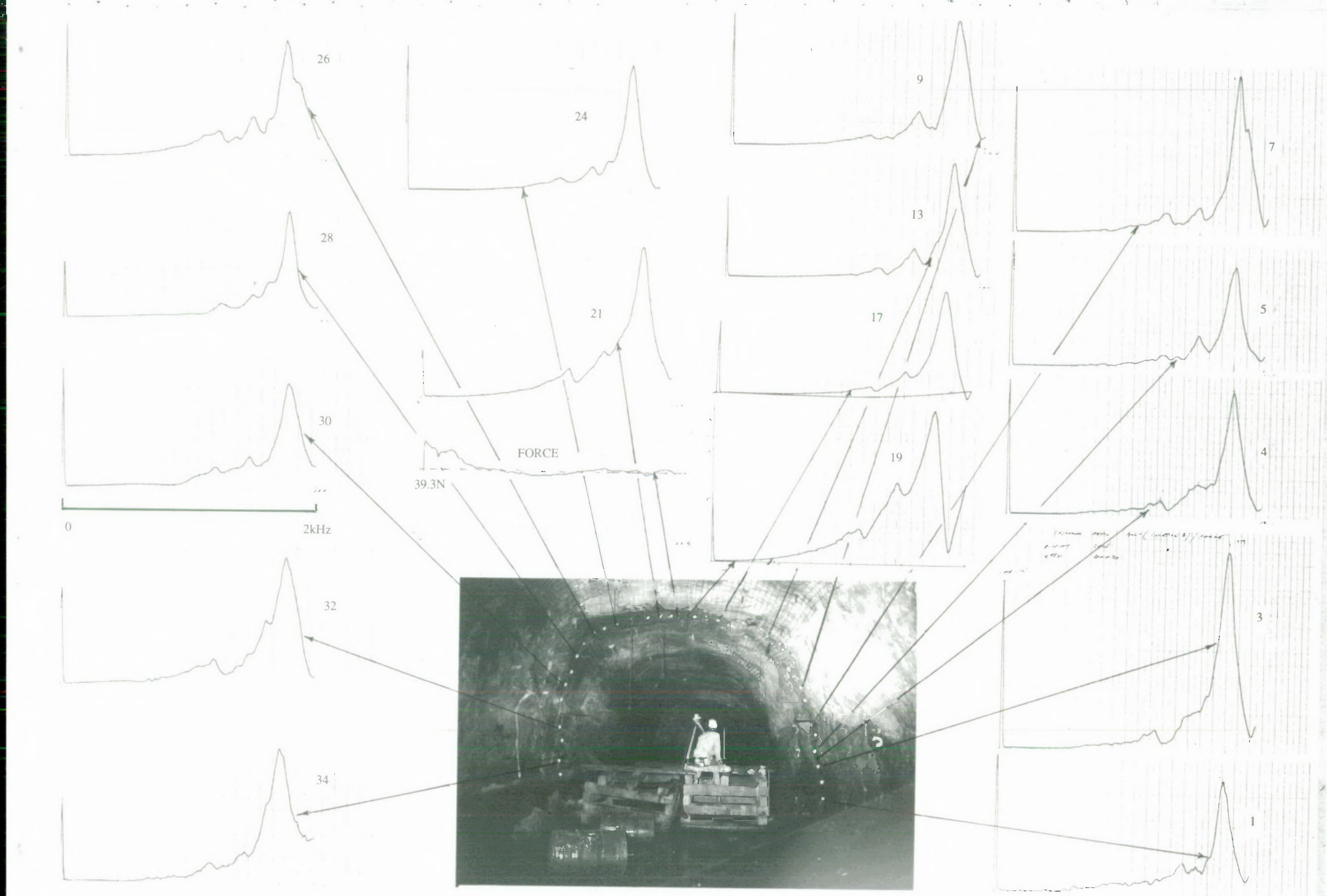
26
24
9
7
28
21
13
5
17
30
FORCE
19
4
39.3N
0
2kHz
32
3
34
1

spectrum was substantially flat over this frequency range. The uncertainty in peak positions was of the order of ± 5 Hz.

Figures 44(a) to (c) presents the modal response of the test cross section at the above frequencies. If a longitudinal wave velocity of 4730 m/s is assumed, based on the average dynamic elastic properties determined in the laboratory tests, then the frequencies of 1200, 1480 and 1790 Hz correspond to dimensionless wavenumbers, k_1a, of 3.6, 4.4 and 5.4 respectively (the radius, a, of the test cross-section is 2.26m, determined photographically from a circle of equal area). These wavenumbers correspond approximately to the 8th, 9th and 11th normal-modes of a cavity in an elastic medium with Poisson's ratio of 0.1. However, these correspondences are only tentative and as revealed by the distorted modal behaviour the idealised theoretical models may not be appropriate to the rock at the test site (there was some evidence at the test site of a textural boundary in the rock fabric in the crown of the heading (S.Matthews, private communication).

Theoretical (acceleration / input force) amplitude transfer functions at the source, for a cavity in an elastic medium with Poisson's ratio equal to 0.1, are presented in Figure 45(a) together with the experimental amplitude data for an accelerometer location near the source (location 19) at the Broken Hill test site, Figure 45(b). For comparison, an experimental amplitude transfer function at a point close to the source is presented in Figure 45(c) from the Hillgrove site where the cavity radius was approximately 1.4 m. Wavenumbers were calculated using the elastic constants quoted by Blair (1975). At the latter site a smaller shaker (Bruel and Kjaer Model 4810) was used as the excitation source, which again, produced a substantially flat force input over the experimental frequency range.

Figures 46(a) to (c) present the phase transfer functions corresponding to amplitude data presented in Figures 45(a) to (c). (The experimental phase responses were plotted

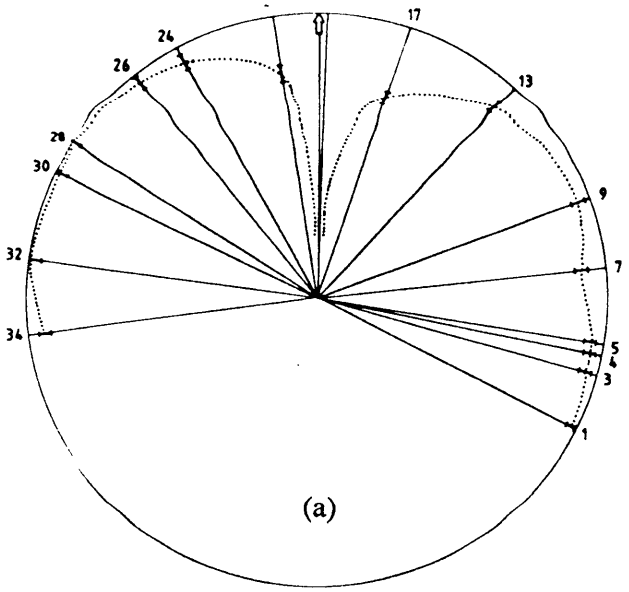

(a)

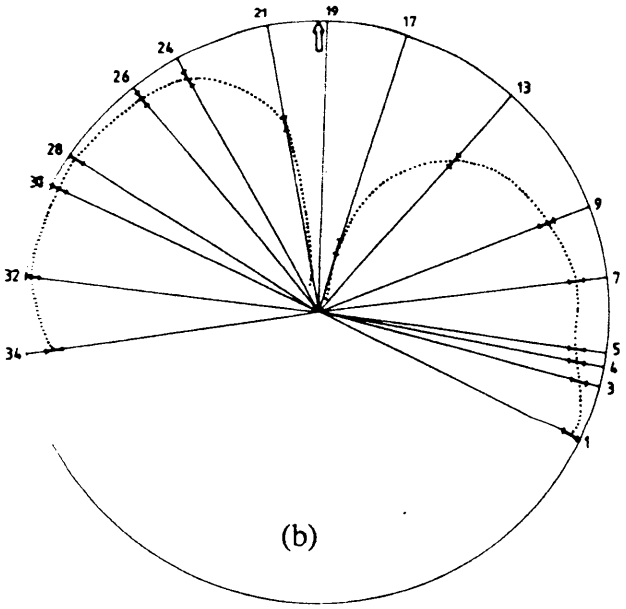

(b)

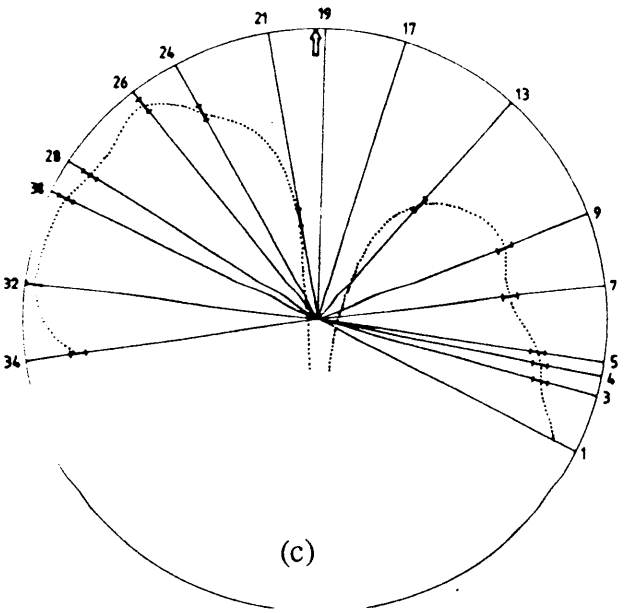

(c)

Figure 44. Modal behaviour of the test cross-section; (a) 1200 Hz, $k_1a = 3.6$, (b) 1480 Hz, $k_1a = 4.4$, (c) 1790 Hz, $k_1a = 5.4$.

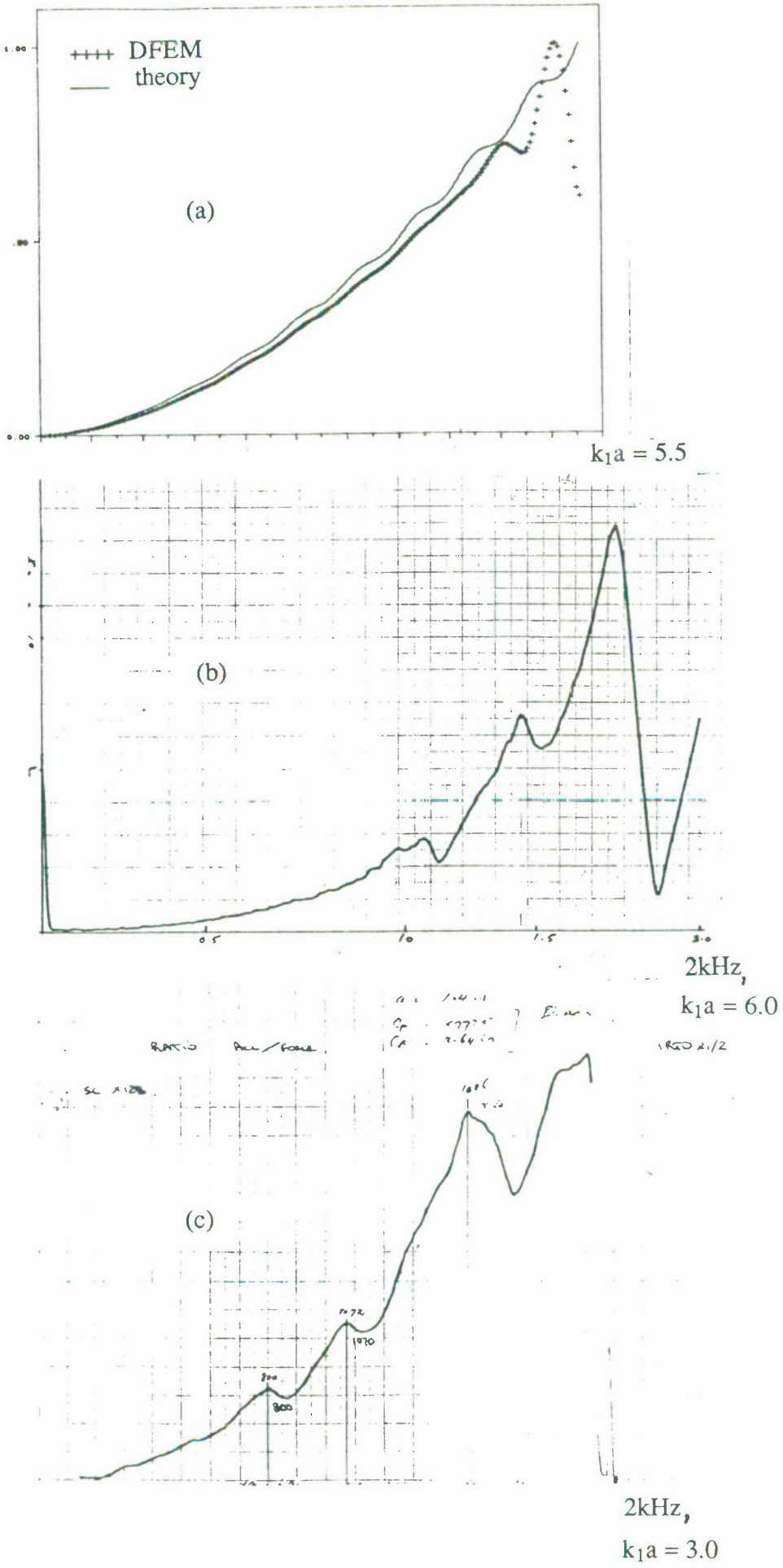

Figure 45. A comparison of theoretical and experimental amplitude transfer functions (acceleration/force); (a) theory and DFEM, (b) Broken Hill test site, (c) Hillgrove tunnel site.

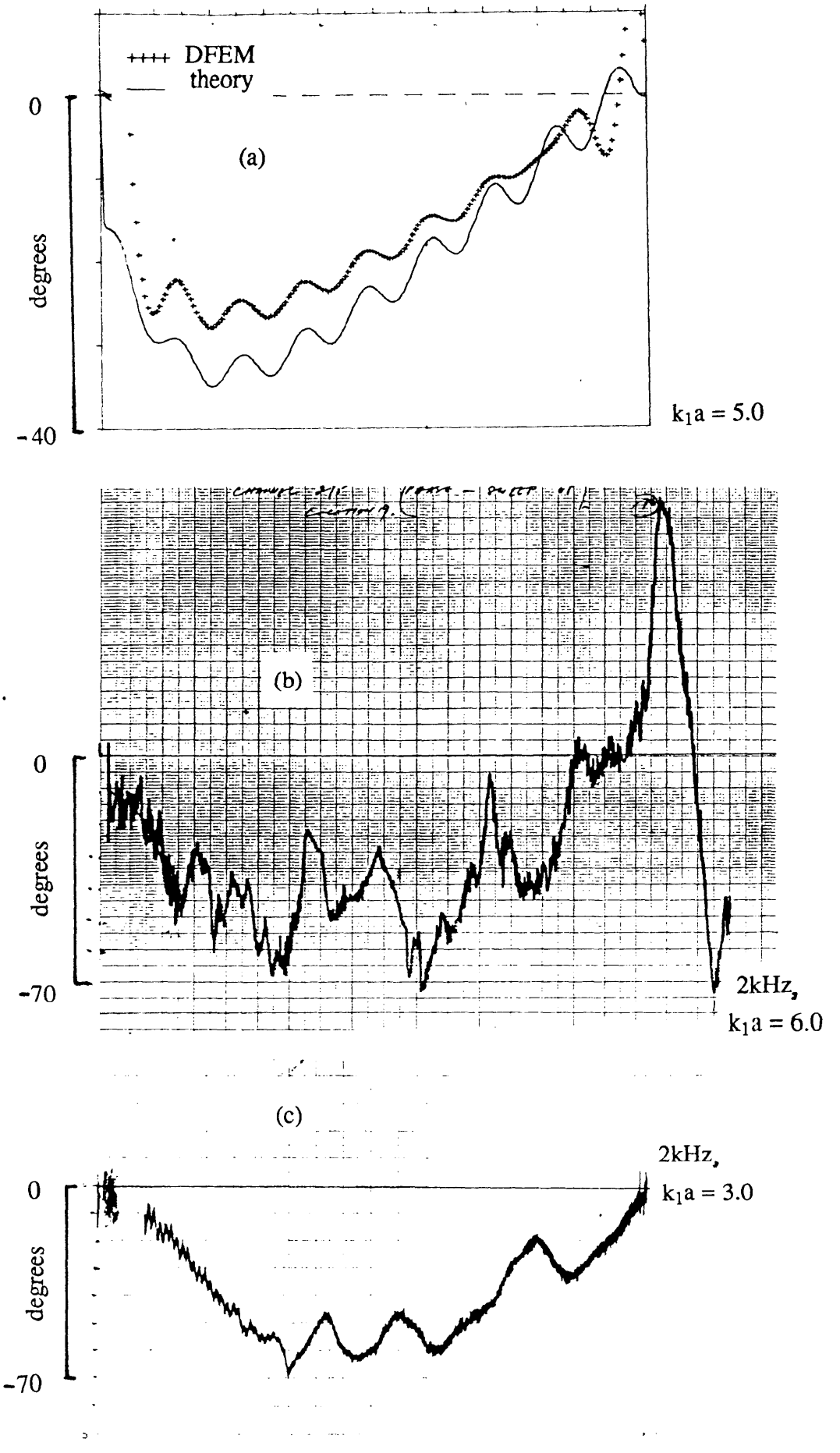

Figure 46. A comparison of theoretical and experimental phase transfer functions (acceleration/force); (a) theory and DFEM, (b) Broken Hill test site, (c) Hillgrove tunnel site.

from tape-recorded data using a CSIRO constructed phase meter). The phase-data obtained at the Broken Hill site appear to be noisy; however, it was repeatable and there is some indication of the 10 oscillations in phase expected for k_1a = to 5.4 ($n \cong 11$) although comparisons with the corresponding theoretical curves are, at best, speculative.

The phase data obtained from Hillgrove shows 5 oscillations which is in agreement with the theoretical predictions for k_1a, 0 to 3.0.

Thus, the experimental cavity responses showed similar behaviour at two widely separated sites; there is clear evidence of resonance behaviour due to circulating Rayleigh type waves, although the response at both sites departed considerably from the predictions of the idealised models.

9. Conclusions

9.1 The roots of the frequency equation for cylindrical cavities in elastic media

The response of a cylindrical cavity in an elastic medium is affected by complex singularities of the cavity transfer functions. Essentially the same denominator, with the same zeros, occurs in a variety of transfer functions described in the literature. An improved method, based on a continued-fractions expansion of Hankel function ratios, has been developed to calculate the zeros of the denominator, i.e., the poles of the transfer function. This method of evaluating the poles is simpler than those used previously and seems to be numerically more stable.

9.2 Analytical and dynamic finite-element models of the line-source/cavity interaction

The complex compliances of the cavity, predicted in both analyses, exhibit mild oscillatory behaviour as a function of wavenumber which is characteristic of lossy resonant systems. The lossy resonances can be attributed to standing surface waves. For a borehole within a rock (or elastic solid) with Poisson's ratio of 0.1, the first three dimensionless wavenumbers, k_1a, at which resonant amplifications occur are 0.288, 0.836 and 1.403. These wavenumbers are approximately equal to the real part of the first three Rayleigh eigenvalues of the frequency equation for cylindrical cavities in elastic media.

The performance of the DFEM model was poorer than expected due to spurious oscillations in the waveforms at long times, most probably arising from inter-element reflections. Nevertheless, the salient features of the analytical model are reproduced. It appears that 48, 4-node, constant strain elements around the semi-cavity are sufficient to

model the cavity compliance amplitude transfer-function up to k_1a =3 to within 4% accuracy. This accuracy becomes 7% when both amplitude and phase are considered.

Undoubtably higher accuracy could be achieved using finer meshes . However, the results presented here give sufficient accuracy to justify the use of DFEM models for cavities of arbitrary shape.

Cavity mode-shapes at resonance, predicted by both analytical and DFEM models, are in good agreement. The mode shapes can be considered to arise from standing Rayleigh-type surface waves.

The transfer functions calculated should be useful for geophysical and non-destructive testing applications involving circumferentially propagating elastic waves.

9.3 Experimental results

All experiments, both in laboratory and field, showed clear evidence for the presence of circulating Rayleigh-type waves on the cavity walls. The dispersive nature of the Rayleigh wave propagation was demonstrated in the laboratory work where it was possible to show good agreement with theory, both pulse travel times and modal response. There was some unexpected asymmetry present in the bore-hole response which may be the result of material inhomogeneity in the granite block or stress-velocity effects although the latter appears unlikely.

The resonances and associated modal behaviour observed in the field showed evidence of the poor quality of the rock at these sites although the response at these sites reproduced the essential features of the theoretical models.

In general, it appears that the experimental resonance peaks associated with circulating Rayleigh-type waves are of higher amplitude than those predicted in the 2-dimensional theoretical models. The phase spectra also show larger variations than the theoretical models near resonance frequencies. This may well be a feature of the 3-dimensional nature of the experimental work and is supported by Lamb's (1904) discussion concerning the response of a half-space to a surface point source. Lamb noted that the separation between P, S and Rayleigh pulses is expected to be more clearly defined in comparison to the 2-dimensional case. The implication is that the resonances will be sharper in the three-dimensional case since the peak-broadening in the two-dimensional case is associated with overlapping modes. This enhanced resonant behaviour bodes well for non-destructive testing applications.

10. Suggestions for further work

1. A solution method should be developed for extraction of the Viktorov poles (normal modes) for the 3-dimensional case of a point source on a cavity wall in an infinite elastic medium. Preliminary work on the denominator (determinant of the equations arising for cavity wall displacements) of the Fourier-Bessel transfer function for this case suggests that each Viktorov pole trajectory (in the 2-dimensional case) will be extended to a surface with the additional poles arising from propagation down the bore-hole axis. These axial modes will, most probably, be more lossy than the circumferential Rayleigh modes.

2. A 3-dimensional DFEM study of the near-field, point source/cavity interaction could be made although costs, in terms of computer processing time, may be prohibitive. The DFEM models can be readily extended to cavities of arbitrary cross-section within heterogeneous rock. Thus, a case study could be made of such a cavity and the influence of cavity geometry could be investigated.

3. A first-order perturbation analysis of the influence of defects on the dynamic behaviour of underground openings has been described by Siggins and Enever (1979). Aspects of this approach could be incorporated into the models described in this thesis. This should then result in a powerful tool for monitoring structural changes via resonance changes in underground mining environments subject to changing stress conditions.